VETOR

# Numerical Simulation of Non-Isothermal Flows in Shale Gas Reservoirs Considering Heating☆

## Simulação Numérica de Escoamentos Não Isotérmicos em Reservatórios de *Shale Gas* Considerando Aquecimento

Lucas Barros Lima[1], Elísio da Costa Nhuta[1], Grazione de Souza[1†], Helio Pedro Amaral Souto[1]

[1] *Instituto Politécnico, Universidade do Estado do Rio de Janeiro, Nova Friburgo, Brasil*
[†]**Corresponding author:** gsouza@iprj.uerj.br

**Abstract**

This study applies the Finite Volume Method to model non-isothermal flow in shale gas reservoirs, accounting for adsorption and gas slippage effects. The analysis focuses on enhanced recovery through the use of static heaters. The proposed model incorporates temperature-dependent absolute permeability and pressure- and temperature-dependent adsorption. A fully implicit formulation is adopted, with linearization via the Picard method and solution of the resulting systems using the Conjugate Gradient method. The results demonstrate that thermal stimulation significantly improves shale gas production. In long-term scenarios, the use of eight heaters increased cumulative production by up to 24% compared to the case without heating. Additionally, the analysis of different heating rates revealed that the 80 kW scenario provides the most favorable performance, achieving a positive energy balance after approximately 1900 days and exceeding 30% efficiency gain over a 40-year period. These findings highlight the importance of thermal effects, adsorption, and slippage in non-isothermal shale gas flow, providing valuable insights for optimizing recovery strategies and improving the economic viability of thermal methods.

**Keywords**

Adsorption • Non-isothermal flow • Reservoir simulation • Shale gas • Slippage

**Resumo**

Este estudo aplica o Método dos Volumes Finitos para modelar o escoamento não isotérmico em reservatórios de gás de folhelho, considerando os efeitos de adsorção e escorregamento do gás. A análise concentra-se na recuperação avançada por meio do uso de aquecedores estáticos. O modelo proposto incorpora a permeabilidade absoluta dependente da temperatura, bem como a adsorção dependente da pressão e da temperatura. Uma formulação totalmente implícita é adotada, com linearização pelo método de Picard e solução dos sistemas resultantes por meio do método dos Gradientes Conjugados. Os resultados demonstram que a estimulação térmica melhora significativamente a produção de gás de folhelho. Em cenários de longo prazo, o uso de oito aquecedores aumentou a produção acumulada em até 24% em comparação com o caso sem aquecimento. Além disso, a análise de diferentes taxas de aquecimento revelou que o cenário de 80 kW apresenta o desempenho mais favorável, atingindo balanço energético positivo após aproximadamente 1900 dias e superando um ganho de eficiência de 30% ao longo de um período de 40 anos. Esses resultados destacam a importância dos efeitos térmicos, da adsorção e do escorregamento no escoamento não isotérmico de gás de folhelho, fornecendo *insights* valiosos para a otimização de estratégias de recuperação e para a melhoria da viabilidade econômica de métodos térmicos.

**Palavras-chave**

Adsorção • Escoamento não isotérmico • Simulação de reservatórios • *Shale gas* • Escorregamento

☆This article is an extended version of the work presented at the XXVIII National Meeting on Computational Modeling (ENMC) & XVI Meeting on Science and Technology of Materials (ECTM), held in Montes Claros, Brazil, October 21–24, 2025.

# 1 Introduction

The shift to cleaner energy sources such as natural gas is vital for mitigating global warming, especially given the projected increase of 2.5 billion in the urban population by 2050 [1], which is expected to drive energy demand. Natural gas offers lower emissions than coal and oil and serves diverse applications [2]. While cleaner than conventional fuels, unconventional extraction, particularly shale gas [3], necessitates mitigation technologies such as Carbon Capture and Storage (CCS) to reduce environmental impacts [4], alongside the continued development of renewable energy sources [5].

Shale gas, natural gas contained within sedimentary shale rock, has become a significant production source, led by the United States of America. Optimizing its extraction requires numerical simulation and reservoir engineering [6] due to the uniquely low permeability and porosity of shale formations [7], where gas is trapped in fractures.

Reservoir engineering and numerical simulation are crucial for understanding and enhancing shale gas extraction [8]. Accurate modeling of adsorption [9] and non-Darcy effects such as gas slippage [10, 11], which are important in low-permeability rocks, is essential for efficient extraction design [12]. Hydraulic fracturing enables shale gas production by creating flow pathways [13], although environmental concerns exist and can be mitigated by proper execution [14]. Thus, understanding gas flow in shale formations while considering these factors is key to optimizing shale gas recovery in both economic and environmental terms.

Thermal methods are increasingly used to enhance shale gas recovery by releasing adsorbed gas through heating [15]. This study focuses on static heaters and their impact on non-isothermal flow. *In situ* heating, used in Enhanced Oil Recovery (EOR) [16], can increase shale gas production by freeing adsorbed gas [17]. Temperature also influences absolute permeability [18], which is a critical factor in thermal recovery optimization. While combustion is another thermal method studied for enhanced recovery [19], non-isothermal flow in shale gas reservoirs involves complex coupled processes such as adsorption and diffusion, in which temperature distribution significantly impacts production [19], highlighting the value of simulation in optimizing thermal recovery.

# 2 Governing Equations

In this work, we advanced toward building a numerical simulator to solve the governing equations of non-isothermal gas flow in a shale gas reservoir, drawing upon elements present in models reported in the literature. This approach enables the investigation of the combined physical effects of gas adsorption and slippage during thermal energy injection via static heaters, with the aim of enhancing production. Thus, absolute permeability is considered a function of temperature, $\mathbf{k}(T)$ [19], and the pressure- and temperature-dependent adsorption phenomenon is assumed, as discussed in [15]. Therefore, the development of this computational tool should allow for a discussion of the combined effects of these physical phenomena on flow behavior, analyzing improvements in production due to the application of static heaters.

The physical-mathematical model adopted in this work incorporates the following assumptions. The flow is considered non-isothermal, two-dimensional in the $xy$-plane, single-phase, and transient. Local thermal equilibrium is assumed to exist between the rock and the fluid. A thermal energy source term, representing volumetric heat generation, is included in the model. The porous medium is considered slightly compressible with constant compressibility and is initially homogeneous and anisotropic with respect to absolute permeability. The porous medium is assumed to be free of connate (irreducible) water, being fully saturated only by hydrocarbons in the gaseous phase. A mass sink term, representing a production well, is incorporated. The fluid, dry natural gas, is considered Newtonian, compressible, and of constant composition. Gas adsorption on the rock matrix is taken into account, while chemical reactions are neglected. Inertial and turbulent effects, as well as thermal exchanges by radiation and hydrodynamic dispersion, are considered negligible. Electrokinetic effects are also disregarded, and the occurrence of gas slippage is accounted for in the flow description.

To account for the influence of temperature, the approach based on the work of [18] was adopted. Thus, the principal components of the absolute permeability tensor, $k\,(T,t)$, are calculated as proposed in [19]

$$k\,(T,t) = \underbrace{\max}_{t\geq 0} \min\left\{\exp\left[\frac{T-T_{res}}{350}\ln(5)\right]k_{ini}, 5k_{ini}\right\}, \tag{1}$$

where $T$ is the temperature, $t$ is the time, $k_{ini}$ is the initial absolute permeability and $T_{res}$ is the initial reservoir temperature.

## 2.1 Conservation of mass

Starting from the continuity equation and Darcy's law, modified to account for non-Darcy effects such as gas slippage, a governing equation for the reservoir pressure can be derived [20]:

$$\left(\Gamma'_p + \Gamma'_{p,ads}\right)\frac{\partial p}{\partial t} - \nabla\cdot\left(\frac{\mathbf{k}_a}{B_g\mu_g}\nabla p\right) - \underbrace{\left(\Gamma'_T + \Gamma'_{T,ads}\right)\frac{\partial T}{\partial t} + \frac{q_{sc}}{V_b}}_{=S_m} = 0, \tag{2}$$

where, for more compact notation, the following coefficients are introduced:

$$\Gamma'_p = \left[\frac{\phi^0 c_\phi}{B_g} + \phi\frac{\partial}{\partial p}\left(\frac{1}{B_g}\right)\right], \tag{3}$$

$$\Gamma'_{p,ads} = \left[\frac{V_{ads}\rho_s^0 c_\rho}{B_g} + \rho_s V_{ads}\frac{\partial}{\partial p}\left(\frac{1}{B_g}\right) + \frac{\rho_s}{B_g}\frac{V_L K(T)}{\left(1+K(T)p\right)^2}\right], \tag{4}$$

$$\Gamma'_T = \left[\frac{\phi^0 c_{\phi T}}{B_g} - \phi\frac{\partial}{\partial T}\left(\frac{1}{B_g}\right)\right], \tag{5}$$

$$\Gamma'_{T,ads} = \left[\frac{V_{ads}\rho_s^0 c_{\rho T}}{B_g} - \rho_s V_{ads}\frac{\partial}{\partial T}\left(\frac{1}{B_g}\right) - \frac{\rho_s}{B_g}\frac{V_L K(T)p}{\left(1+K(T)p\right)^2}\left(-\frac{1}{2T} + \frac{E_{ads}}{RT^2}\right)\right], \tag{6}$$

where the superscript "0" denotes reference values; $p$ is the pressure; $\mathbf{k}_a$ denotes the apparent permeability tensor; $B_g = \rho_{sc}/\rho_g$ is the formation volume factor; the superscript "sc" denotes standard conditions; $\rho_g$ is the gas density; $\mu_g$ is the gas viscosity; $q_{sc}$ is a source term; $V_b$ is the bulk volume; $\phi$ is the porosity; $c_\phi$, $c_{\phi T}$, $c_\rho$ and $c_{\rho T}$ are the rock and shale formation compressibility and thermal expansion coefficients, respectively; $\rho_s$ is the shale formation density; $V_{ads}$ is the adsorbed specific volume; $V_L$ is the Langmuir volume; $K(T)$ is the adsorption coefficient; $E_{ads}$ is the characteristic adsorption energy; and $R$ is the universal gas constant [20].

Now, the apparent permeability tensor is introduced as [10],

$$\mathbf{k}_a = \left(1 + \frac{4K_n}{1+K_n}\right)\mathbf{k} \tag{7}$$

where $K_n = \lambda/R_h$ is the Knudsen number and

$$\lambda = \frac{\mu_g}{p}\sqrt{\frac{\pi ZRT}{2M}}, \tag{8}$$

$$R_h = 2\sqrt{2\tau}\sqrt{\frac{k_m}{\phi}} \tag{9}$$

represent the mean free path of the molecules and a characteristic length of the porous medium [10, 11], with $Z$ being the compressibility factor; $M$ the molecular mass; $\tau$ representing the porous medium tortuosity; and $k_m$ the geometric mean of the principal absolute permeabilities. In the case of the derivatives of $B_g^{-1}$, the calculation should be performed using numerical approximations [21].

## 2.2 Energy conservation

In this study, the assumption of local thermal equilibrium is adopted, characterized by the equality between the average temperatures of the fluid ($T_g$) and the rock ($T_s$). This methodological choice contrasts with the approach taken by [22], which is based on the premise of local thermal non-equilibrium. It should be emphasized that this represents a specific case of the more general model introduced by [23] and that, under certain hypotheses, it can be applied in practice [24]. Therefore, by setting $T_g = T_s = T$, it is possible to obtain a one-equation model [23, 24]. Hence, the energy equation employed here is given by:

$$\frac{\partial}{\partial t}(\rho c_p T) - \nabla\cdot(\boldsymbol{\kappa}\nabla T) \underbrace{+\nabla\cdot\left(\rho_g h_g \mathbf{v}\right) - \frac{q_H}{V_b} - \frac{\rho_{sc,g} q_{sc} h_g}{V_b}}_{=-S_T} = 0, \tag{10}$$

where $\mathbf{v}$ is the superficial velocity and $\boldsymbol{\kappa}$ is the effective thermal dispersion tensor, considering the contribution of thermal conductivity and excluding those of tortuosity and hydrodynamic dispersion [23],

$$\boldsymbol{\kappa} = \phi\boldsymbol{\kappa}_g + (1-\phi)\boldsymbol{\kappa}_s, \tag{11}$$

where $\boldsymbol{\kappa}_g$ and $\boldsymbol{\kappa}_s$ are the thermal conductivities of the fluid and the rock,

$$\rho c_p = \phi\left(\rho_g c_{pg}\right) + (1-\phi)\left(\rho_s c_{ps}\right), \tag{12}$$

$q_H$ is the volumetric thermal source provided by the heaters, $h_g = c_{pg} T_g$ is the enthalpy, and $c_p$ is the specific heat.

### 2.3 Initial and boundary conditions

A phenomenon described by parabolic partial differential equations is incomplete unless appropriate initial and boundary conditions are provided. Therefore, for the problem to be mathematically well posed, the initial pressure and temperature of the reservoir are prescribed throughout its domain at a given arbitrary initial time, that is,

$$p(x, y, T, t = 0) = p_0(x, y, T), \tag{13}$$

$$T(x, y, p, t = 0) = T_0(x, y, p). \tag{14}$$

Regarding the boundary conditions, a no-flow condition is considered at the reservoir boundaries, that is, at $x = 0$ and $y = 0$, and at $x = L_x$ and $y = L_y$:

$$\left(\frac{\partial p}{\partial x}\right)_{x=0,L_x} = \left(\frac{\partial p}{\partial y}\right)_{y=0,L_y} = 0, \tag{15}$$

$$\left(\frac{\partial T}{\partial x}\right)_{x=0,L_x} = \left(\frac{\partial T}{\partial y}\right)_{y=0,L_y} = 0, \tag{16}$$

where $L_x$ and $L_y$ represent the length and width of the reservoir, respectively, and its height is $L_z$.

Furthermore, the prescribed production rate from the well (of length $L_{wf}$) is imposed via a mass source term [25]

$$q_{sc} = -J_w\left(p - p_{wf}\right), \tag{17}$$

where $J_w$ is the productivity index and $p_{wf}$ is the bottomhole flowing pressure. Equation (17) allows the calculation of the well pressure once its flow rate is prescribed, and vice versa.

## 3 Numerical Methodology

The Finite Volume Method (FVM) originates from the integral formulation of conservation laws, which grants it several advantages [26]. Among these benefits, its ability to preserve conserved quantities, such as mass, momentum, and energy, throughout the domain discretization process stands out, contributing to numerically stable and conservative solutions.

The domain is then partitioned into finite volumes, and the governing equations are integrated over each of these volumes and in time, resulting in a system of algebraic equations. The approximate solution of this system, obtained using the Conjugate Gradient Method, provides the desired pressure and average temperature fields.

Following the nomenclature commonly adopted in the literature [26], the uppercase subscripts $W$ (West), $E$ (East), $S$ (South), and $N$ (North) indicate the neighboring nodes to the central node $P$, while the lowercase subscripts ($w$, $e$, $s$, and $n$) indicate the corresponding faces of the central finite volume in each direction. The structured mesh consists of $n_x$ and $n_y$ finite volumes in the $x$- and $y$-axis directions, respectively, with spatial increments equal to $\Delta x$ and $\Delta y$. The time increment is denoted by $\Delta t$.

After integrating the governing equations over a finite volume and in time, from $t^n$ (old) to $t^{n+1}$ (new), employing fully implicit time formulations, three-point centered differences for the spatial derivatives, and conservative expansions for the accumulation terms [21], the final discretized forms are obtained [20]. Regarding the equation for determining pressure:

$$\Lambda_P p_P^{new} = \Lambda_e p_E^{new} + \Lambda_w p_W^{new} + \Lambda_n p_N^{new} + \Lambda_s p_S^{new} + (S_m)_P^{new} + \left(\Gamma_p + \Gamma_{p,ads}\right)_P^{new} p_P^{old}, \tag{18}$$

where the different coefficients are given by

$$\Lambda_P = \left(\Gamma_p + \Gamma_{p,ads}\right)_P^{new} + \Lambda_e + \Lambda_w + \Lambda_n + \Lambda_s, \tag{19}$$

$$\Lambda_e = \left(\frac{k_{ax}\Delta y_P L_z}{B_g \mu_g \Delta x_e}\right)_e^{new}, \qquad \Lambda_w = \left(\frac{k_{ax}\Delta y_P L_z}{B_g \mu_g \Delta x_w}\right)_w^{new}, \tag{20}$$

$$\Lambda_n = \left(\frac{k_{ay}\Delta x_P L_z}{B_g \mu_g \Delta y_n}\right)_n^{new}, \qquad \Lambda_s = \left(\frac{k_{ay}\Delta x_P L_z}{B_g \mu_g \Delta y_s}\right)_s^{new}, \tag{21}$$

$$(S_m)_P^{new} = (q_{sc})_P^{new} + \left(\Gamma_T + \Gamma_{T,ads}\right)^{new} \left(T_P^{new} - T_P^{old}\right), \tag{22}$$

where $\Gamma_p = \Gamma'_p V_b/\Delta t$; $\Gamma_{p,ads} = \Gamma'_{p,ads} V_b/\Delta t$; $\Gamma_T = \Gamma'_T V_b/\Delta t$; and $\Gamma_{T,ads} = \Gamma'_{T,ads} V_b/\Delta t$. The terms $\Lambda_e$, $\Lambda_w$, $\Lambda_n$, and $\Lambda_s$ are called transmissibilities, and the properties that must be evaluated at the faces of the finite volumes are calculated using harmonic averages for rock properties and arithmetic averages for fluid properties [22].

Next, the final discretized form of the energy equation is presented:

$$\Phi_P T_P^{new} = \Phi_e T_E^{new} + \Phi_w T_W^{new} + \Phi_n T_N^{new} + \Phi_s T_S^{new} + (S_T)_P^{new} + \frac{\left(\rho c_p V_b\right)_P^{old}}{\Delta t} T_P^{old}, \tag{23}$$

with its coefficients calculated according to the following equations:

$$\Phi_P = \frac{\left(\rho c_p V_b\right)_P^{new}}{\Delta t} + \Phi_e + \Phi_w + \Phi_n + \Phi_s, \tag{24}$$

$$\Phi_e = \left(\frac{\kappa_x \Delta y_P L_z}{\Delta x_e}\right)_e^{new}, \qquad \Phi_w = \left(\frac{\kappa_x \Delta y_P L_z}{\Delta x_w}\right)_w^{new}, \tag{25}$$

$$\Phi_n = \left(\frac{\kappa_y \Delta x_P L_z}{\Delta y_n}\right)_n^{new}, \qquad \Phi_s = \left(\frac{\kappa_y \Delta x_P L_z}{\Delta y_s}\right)_s^{new}, \tag{26}$$

$$(S_T)_P^{new} = (q_H)_P^{new} + \left[\left(\rho_{sc} h_g + B_g p\right) q_{sc}\right]_P^{new} + \varphi, \tag{27}$$

where

$$\varphi = \Lambda_{T,e} p_E^{new} + \Lambda_{T,w} p_W^{new} + \Lambda_{T,n} p_N^{new} + \Lambda_{T,s} p_S^{new} - \left(\Lambda_{T,e} + \Lambda_{T,w} + \Lambda_{T,n} + \Lambda_{T,s}\right) p_P^{new} \tag{28}$$

and

$$\Lambda_{T,\eta} = \left[\left(\rho_{sc} h_g\right) \Lambda\right]_\eta \tag{29}$$

for each direction $\eta = e, w, n, s$.

The numerical solution employs operator splitting [27], sequentially solving linearized algebraic systems for pressure and then temperature. Each solution involves Picard iterations [28], in which coefficients are updated based on values from the previous iteration ($\upsilon$) to calculate the current values ($\upsilon + 1$). For the pressure calculation, the coefficients are evaluated using $p^\upsilon$ and $T^\upsilon$, and the iterations proceed until pressure convergence is achieved within a tolerance ($tol_2$). The temperature calculation follows a similar procedure, using $T^\upsilon$ and the updated $p^{\upsilon+1}$, and iterating until temperature convergence. The inner linear systems for each variable are solved to a tolerance ($tol_1$).

For the problem considered in this work, where there is a vertical producer well of length $L_z$,

$$J_w = \left\{\left(2\pi\sqrt{k_{ax}k_{ay}}L_z\right)\left[B_g\mu_g \ln\left(\frac{r_{eq}}{r_w}\right)\right]^{-1}\right\}_P^{new} \tag{30}$$

where $r_w$ is the well radius and $r_{eq}$ is the equivalent radius [29], having been adapted for use with apparent permeabilities [20], considering the computation of properties in the finite volume that hosts the wellbore.

# 4 Numerical Results

The numerical code was developed in the C programming language using the *Visual Studio Code* editor, version 1.82.2, compiled with `gcc` (*GNU C Compiler*) version 11.4.0, and executed on a GNU/Linux operating system (Ubuntu 22.04.03 LTS).

Tables 1, 2, and 3 provide the values of the properties and parameters used to define the base case, which considers the effects of gas adsorption and slippage. In Table 3, $\gamma$ represents the specific weight of the gas, and is used in the determination of pseudo-critical pressure and temperature, such that the formation volume factor is calculated from the equation of state [30]

$$B_g = \frac{p_{sc}}{p_g}\frac{T_g}{T_{sc}} Z_g(p_g, T_g, \gamma), \tag{31}$$

where the compressibility factor of the gas $Z_g$ is a function of the pressure, temperature, and density of the gas [30].

Table 1: General parameters.

| Parameter | Value | Unit | Parameter | Value | Unit |
|---|---|---|---|---|---|
| $F_{\Delta t}$ | 1.2 | - | $t_{max}$ | 1,464 | day |
| $h_{pos}$ | 20 | m | $tol_1$ | $1\times10^{-5}$ | kPa |
| $L_x = L_y$ | 1,080 | m | $tol_2$ | $1\times10^{-5}$ | K |
| $L_z = L_{wf}$ | 40 | m | $T_{\text{init}} = T^0$ | 400.15 | K |
| $n_x = n_y$ | 185 | - | $x_w = y_w$ | 540 | m |
| $p_{\text{init}} = p^0$ | 45,000 | kPa | $\Delta t_{\text{init}}$ | 0.5 | day |
| $q_{sc}$ | -2,500 | std $m^3$/day | $\Delta t_{\text{final}}$ | 5 | day |

Table 2: Rock Parameters.

| Parameter | Value | Unit | Parameter | Value | Unit |
|---|---|---|---|---|---|
| $c_\phi$ | $1.45\times10^{-6}$ | $kPa^{-1}$ | $k_x = k_y$ | $5\times10^{-18}$ | $m^2$ |
| $c_{\phi T}$ | $5.4\times10^{-6}$ | $K^{-1}$ | $\kappa_r$ | 3.5 | W/(m K) |
| $c_\rho$ | $10^{-6}$ | $kPa^{-1}$ | $\rho_s$ | 3,203.7 | kg/$m^3$ |
| $c_{\rho T}$ | $5.0\times10^{-9}$ | $K^{-1}$ | $\tau$ | 1.41 | - |
| $c_{pr}$ | 1.25604 | kJ/(kg K) | $\phi^0$ | 0.08 | - |

Table 3: Fluid Parameters.

| Parameter | Value | Unit | Parameter | Value | Unit |
|---|---|---|---|---|---|
| $c_{pg}$ | 2.5 | kJ/(kg K) | $R$ | 8.3161 | J/(mol K) |
| $E_{ads}$ | -20.936 | J/mol | $T_{sc}$ | 298.15 | K |
| $K_0$ | $3.2288\times10^{-9}$ | $K^{0.5}$ | $V_L$ | $3.12398\times10^{-5}$ | $m^3$/kg |
| $p_L$ | 1,100 | kPa | $\gamma$ | 0.6 | - |
| $p_{sc}$ | 101.325 | kPa | $\kappa_g$ | 0.075 | W/(m K) |

The simulation begins with an initial time step $\Delta t_{init}$, which is multiplied by the growth factor $F_{\Delta t}$ to determine the subsequent time steps. This procedure continues until the maximum time step, $\Delta t_{\text{final}}$, is reached, after which it remains constant. The total production time is defined as $t_{max}$. Finally, the coordinates defining the well location are given by $(x_w, y_w)$.

The numerical approach was validated against two analytical solutions: one for transient diffusion in pressure and another for dimensionless transient advection-diffusion in temperature, showing good agreement [20]. Mesh refinement studies further confirmed the accuracy of the method, with results converging to a unique solution as the mesh was refined [20].

## 4.1 Enhanced Oil Recovery (EOR) Performance

The performance of static heaters under various shale gas production scenarios is now analyzed. To this end, the pressure at the production well was kept constant at $p_{wf} = 300$ kPa, simulating an operational constraint, and the relationship from [25] was used to calculate the flow rate and production at each time step, that is, $q_{sc} = J_w \left(p - p_{wf}\right)$, corresponding to Eq. (17).

In all scenarios, a maximum allowable average temperature of 680 K was adopted for any cell. It is understood that exceeding this value could lead to gas combustion [19]. Once this limit is reached, the heaters are turned off. In the simulated cases shown in Figs. 1 and 2, where $h_{pos}$ represents the distance between the heaters and the production well and $G_p$ the cumulative production, after the heaters are turned off and the maximum temperature decreases to 670 K, they are turned on again, thus repeating the heating process cyclically. Prescribing the temperature in the heater cell would not be a suitable approach, as it would not be physically realistic due to the model geometry and the lack of a heater-reservoir coupling model.

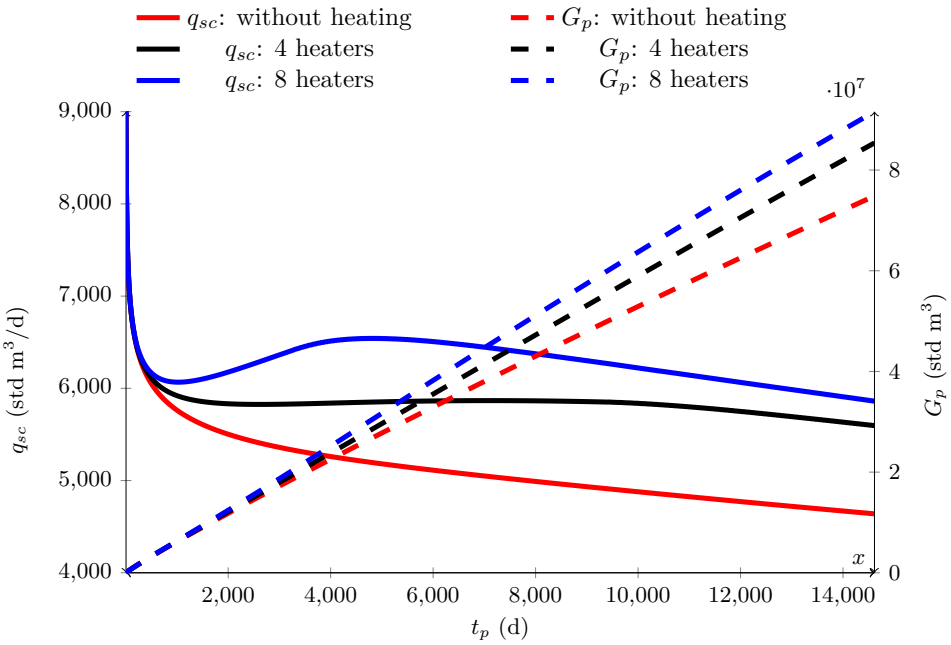


Figure 1: Production rate and cumulative production: Variation in the number of heaters.

Figure 1 shows the results with the heaters positioned 20 m from the production well and evaluates the effect on gas production when using four or eight heaters, as well as without any heating. When comparing the different production configurations over longer durations, it is observed that increasing the number of static heaters leads to a significant attenuation of the flow rate decline, in some cases even reversing it.

This behavior is directly related to the increase in absolute permeability in the heated region and gas desorption driven by the temperature increase. These findings are consistent with results reported in the literature, where thermal stimulation enhances gas desorption and increases apparent permeability in shale formations, leading to improved production performance [17, 19].

The long-term analysis reveals a considerable increase in cumulative shale gas production due to reservoir heating, as illustrated in Fig. 1. The cumulative production curve shows substantial gains with an increasing number of static heaters, with quantitative values presented in Table 4. Recovery using four and eight heaters substantially out-

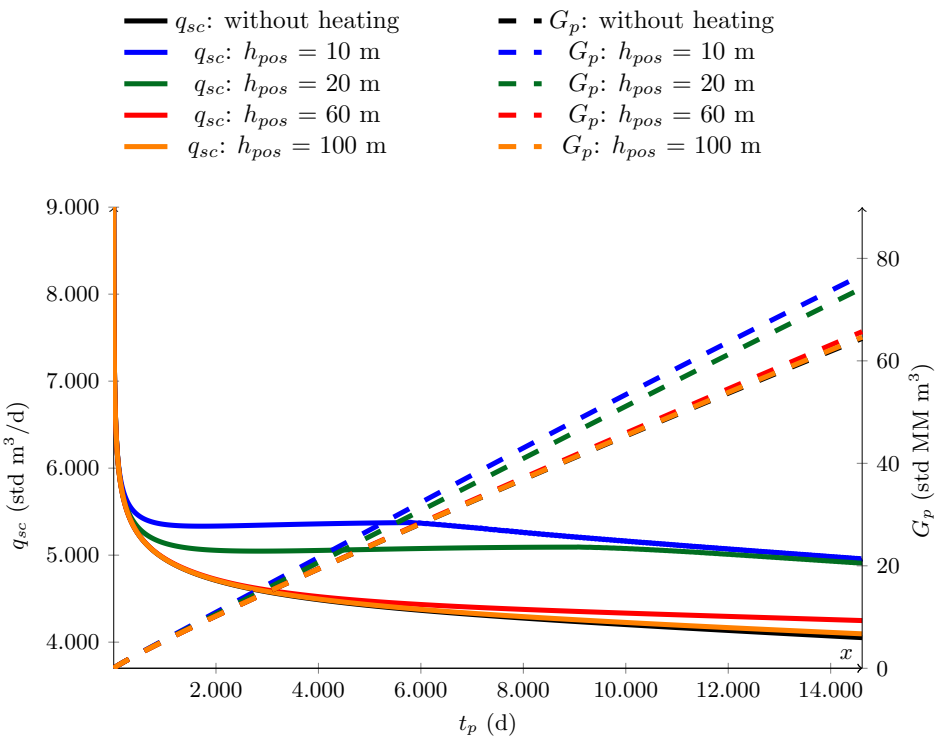


Figure 2: Production rate and cumulative production: Proximity of the heaters.

performs production without employing the thermal recovery method. The positive effect of increased temperature on shale gas production is also highlighted.

Table 4: Production increase by varying the number of heaters.

| Case | $G_p$ (std MM m$^3$) | Production increase |
|---|---|---|
| Without heating | 64.38 | 0% |
| 4 heaters | 74.19 | 15% |
| 8 heaters | 79.73 | 24% |

Although the slippage effect was attenuated due to the adoption of the model proposed by [10], the results indicate that the gains associated with the temperature increase outweigh any reduction, resulting in an overall increase in shale gas production.

However, it can be observed from the cumulative production curve that a significant amount of time may be required to realize any substantial gain associated with the use of the recovery method, as the curves begin to separate after more than 2,000 days of production.

In turn, the results presented in Fig. 2 show that there is an advantage to positioning the heaters as close as possible to the production well. As anticipated, for larger distances, the effect of thermal heating becomes negligible. The observed reduction in effectiveness with increasing distance from the production well is in agreement with previous studies, which indicate that thermal effects are highly localized and strongly dependent on heat transfer efficiency within the reservoir [17, 19].

Moving now to another scenario, whose results are shown in Fig. 3, where SD stands for Shut Down, the effect of not restarting the heaters once the stipulated temperature limit of 680 K is reached is studied. It is noted that, moments after shutdown, the production rate curve abruptly deviates, revealing a situation that characterizes an increase in production from that point onward.

This gain in production rate can be explained by the combination of decreasing pressure and temperature over time, since the reduction in pressure favors gas slippage, which, in turn, is mitigated by the increase in temperature. As shown in Fig. 4, for a heating rate of 50 kW with four heaters positioned 20 m from the production well, shutdown

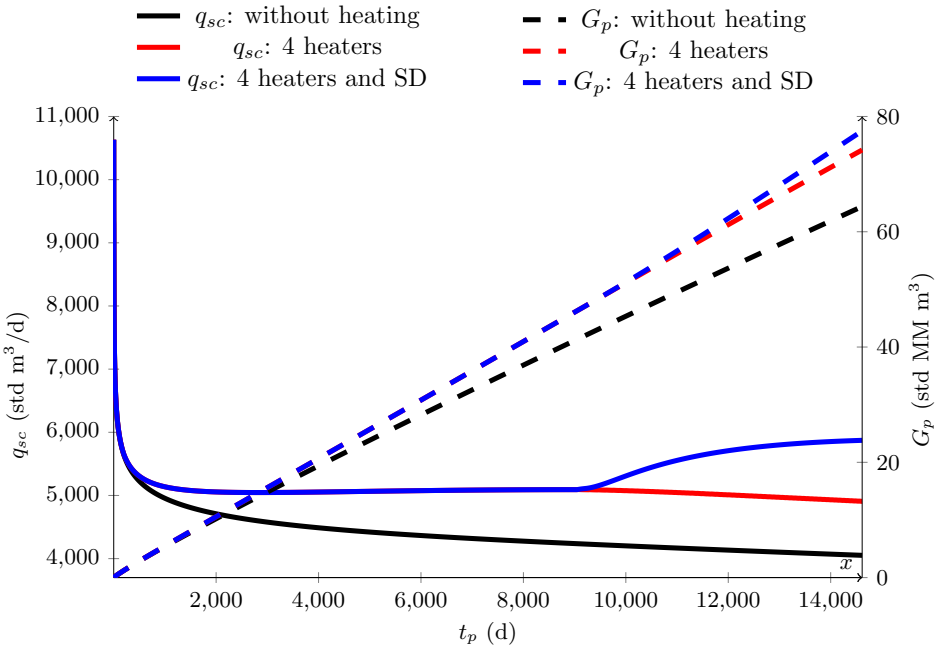


Figure 3: Production rate and cumulative production: Continuous heating.

occurred only after 9,039 days of operation, resulting in a total energy injection of 43.39 GWh into the reservoir, whereas at a heating rate of 80 kW, it was 7.86 GWh in just 1,024 days of production.

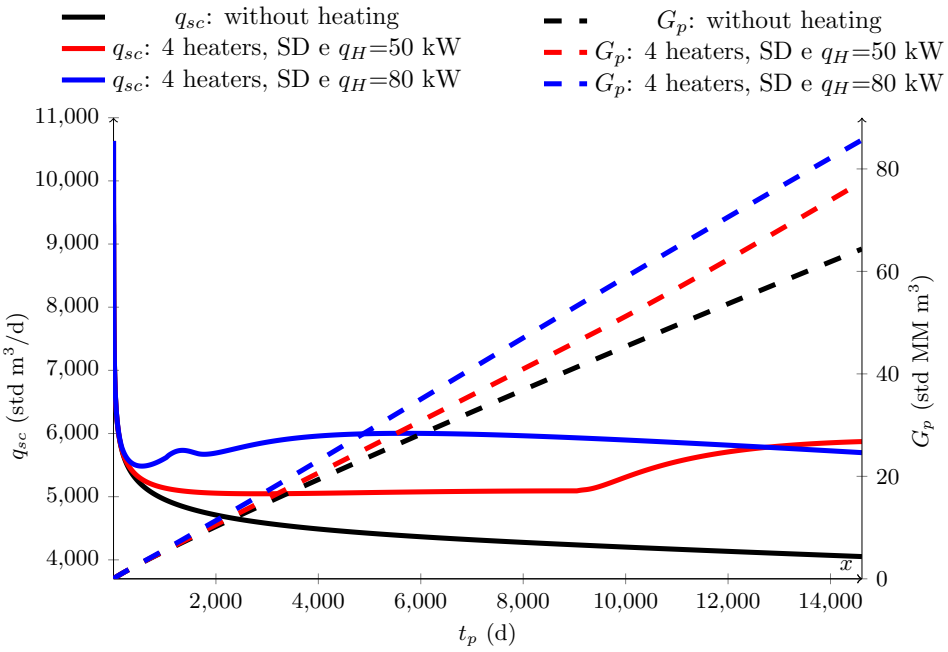


Figure 4: Production rate and cumulative production: Heating off.

Furthermore, considering the balance of the difference between the scenarios with and without heating, it is necessary to account for whether gains were achieved through the use of the recovery method. Thus, considering that 1 m$^3$ of natural gas is equivalent to 36,303 BTU, the balances, converted into energy measured in MMBTU ($10^6$ BTU), were calculated, and the results are presented in Figs. 5 and 6. An efficiency of 70% was assumed for the thermal energy injection operation.

The curve for 100 kW showed that an adjustment is essential when choosing the energy injection rate into the

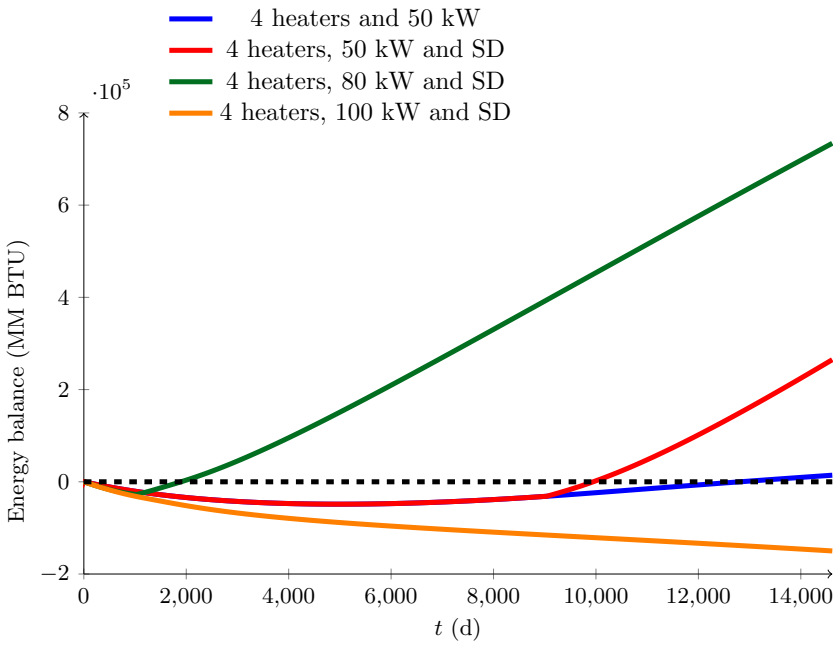


Figure 5: Production rate and cumulative production: Measured in BTU.

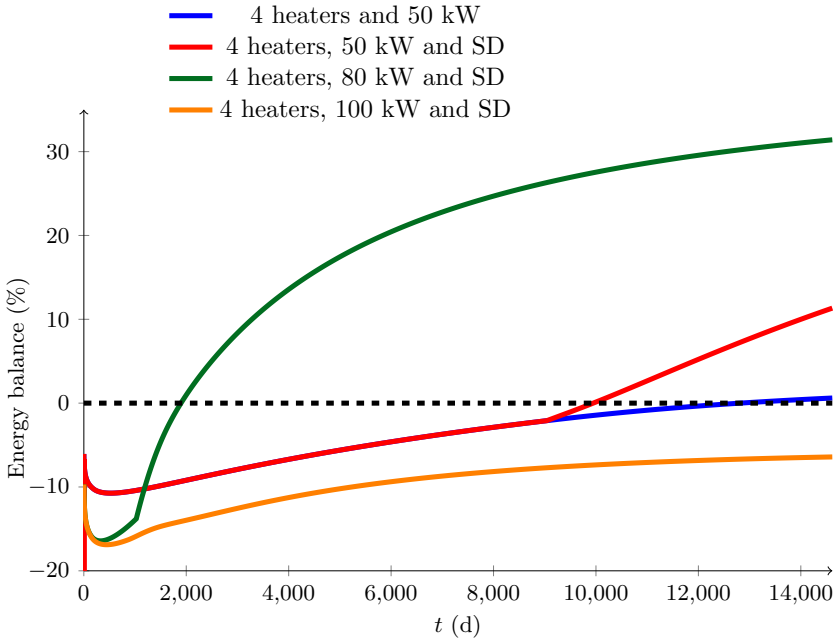


Figure 6: Production rate and cumulative production: Measured in percentage.

system, as it proved to be, by far, the worst case, despite the increased heating rate. Moreover, analyzing Figs. 5 and 6, it is observed that from approximately 1,900 days (more than five years), in the 80 kW heating scenario, a positive energy balance began to occur.

The delayed onset of significant production gains is consistent with the thermal diffusion process in porous media, which typically requires extended periods to effectively propagate heat and impact reservoir properties. This increase continued over the 40 years of operation, resulting in gains exceeding 30% at the end of this period.

In contrast, the other scenarios did not show the same advantage. The analysis revealed that using the thermal energy injection method with 80 kW heating until the target temperature was reached proved to be the most favorable compared to the other evaluated configurations. The identification of an optimal heating rate is consistent with

previous studies on thermal recovery processes, which emphasize that excessive energy input may reduce overall efficiency, highlighting the importance of balancing energy injection and production gains [19].

## 4.2 Sensitivity Analysis

This section presents a sensitivity analysis aimed at evaluating the influence of key operational and physical parameters on the reservoir behavior and production performance. In particular, the effects of variations in production time and thermal stimulation are investigated to assess their impact on pressure and temperature distributions.

### 4.2.1 Production Time

Figures 7, 8, and 9 display the results for reservoir and well pressures, as well as temperature, as functions of production time. It can be observed that, as production time increases, both pressure and temperature are affected, with a notable change in pressure occurring after approximately 2,000 days. Furthermore, a subsequent increase in temperature is observed due to the influence of the static heaters.

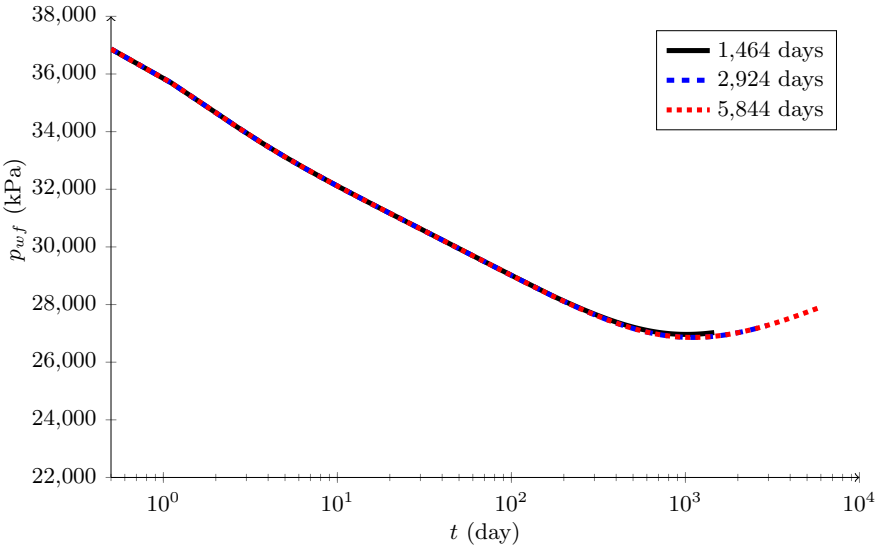


Figure 7: Variation of production time: Well pressure.

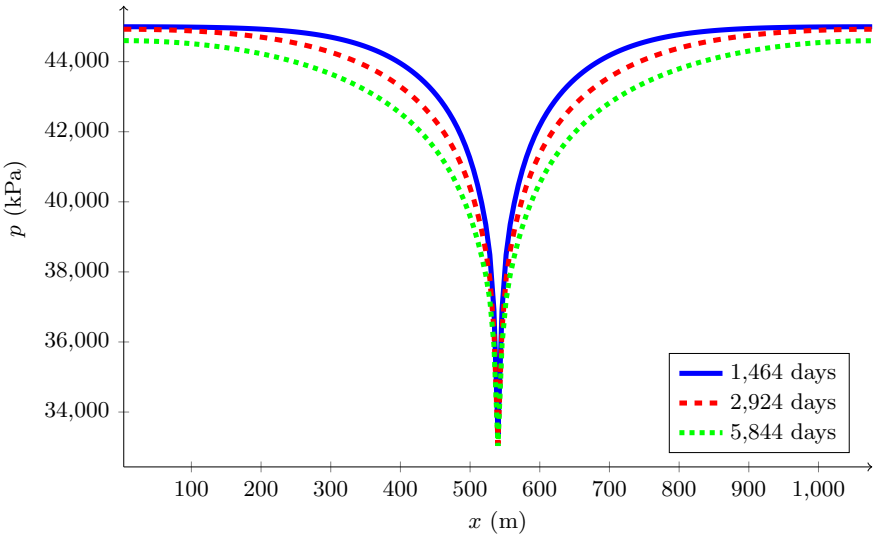


Figure 8: Variation of production time: Reservoir pressure.

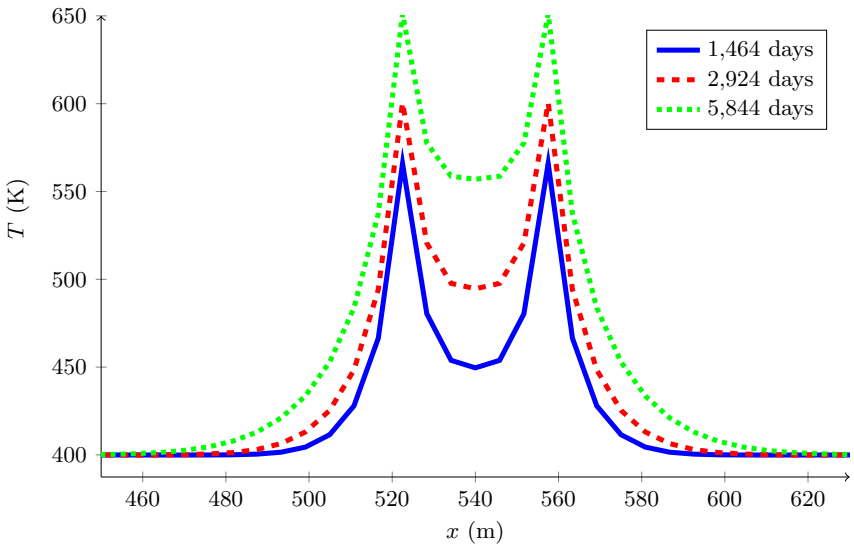


Figure 9: Variation of production time: Reservoir temperature.

### 4.2.2 Heater Wells Placement

The following results were obtained by varying the distance between the heater wells and the producer. Distances of 20, 60, and 100 m from the vertical production well location were considered.

Due to their positioning in the reservoir, the temperature increase affected the pressure in the production well only for the case where the distance was 20 m, over the stipulated production time, as observed in Fig. 10, leading to a smaller pressure drop. From Figs. 11 and 12, it was found that the reservoir pressure was practically unaffected and that the maximum temperatures reached were virtually the same, although only the wells positioned closer to the production well appreciably affected the temperature in the region containing the well.

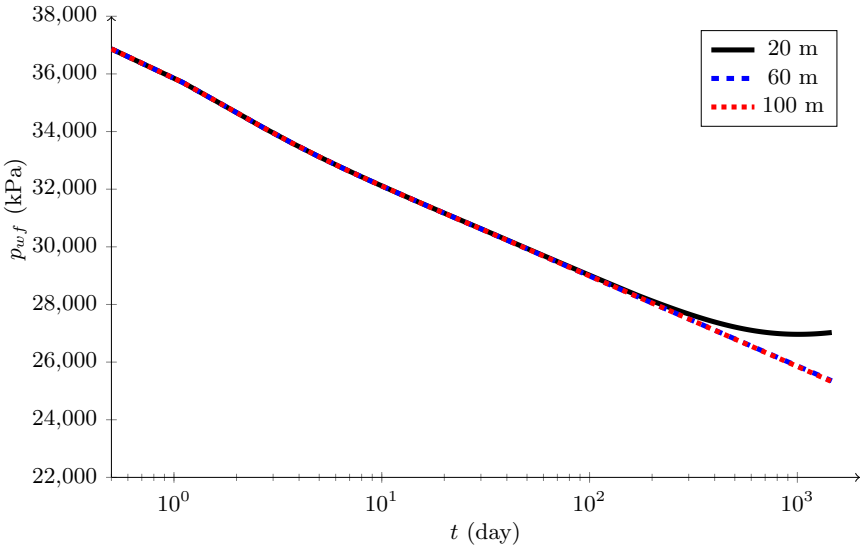


Figure 10: Variation of heater well positioning: Well pressure.

In this case, due to the variation of the absolute permeability as a function of temperature, it is expected to increase in the vicinity of the production well, contributing to a reduction in flow resistance in the aforementioned region.

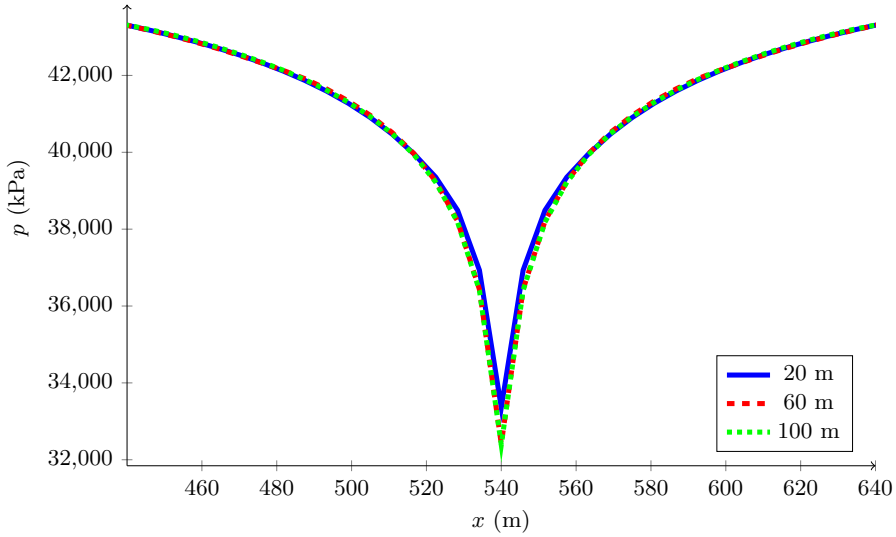


Figure 11: Variation of heater well positioning: Reservoir pressure.

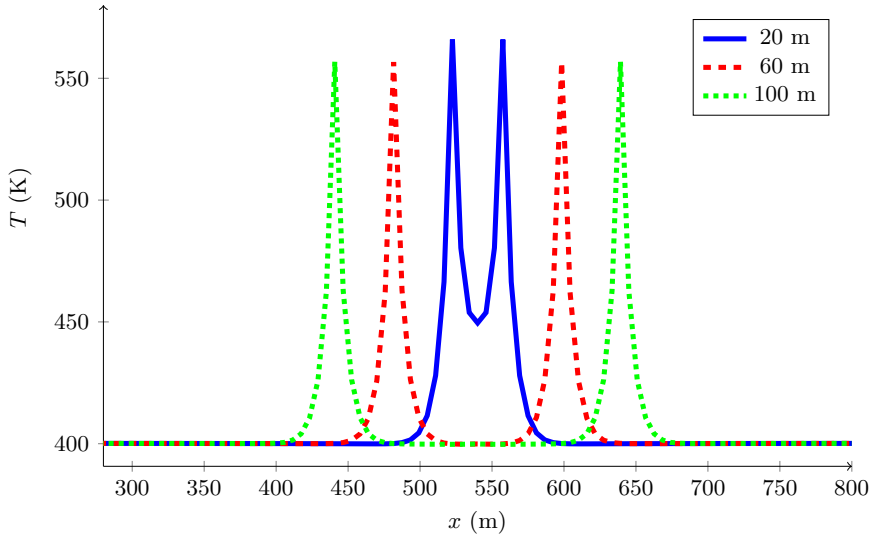


Figure 12: Variation of heater well positioning: Reservoir temperature.

## 5 Conclusions

The results indicate that increasing reservoir temperature as a stimulation method in the near-wellbore region, thereby enhancing absolute permeability in the heated area, can significantly benefit shale gas production in the long term, particularly when the heaters are located close to the production well. The heating rate also plays a crucial role in the efficiency of the recovery process, highlighting the importance of evaluating different production scenarios to achieve tangible gains. However, it is important to note that the benefits associated with this recovery method may take several years to become significant.

From an economic perspective, the feasibility of shale gas reservoir heating projects depends on multiple factors, including operational and installation costs. In this context, the 80 kW heating scenario demonstrated the most favorable cost-benefit ratio, achieving a positive energy balance after approximately 1900 days and resulting in efficiency gains exceeding 30% over long-term operation. These findings reinforce the potential of optimized thermal strategies to improve the practical viability of such recovery methods.

Regarding the analysis of pressure and temperature fields during sensitivity tests, significant variations in bottomhole pressure and temperature profiles were observed over production time. The combined effects led to pressure drops and temperature increases, emphasizing the importance of monitoring and control in long-term operations.

## Acknowledgements

This study was financed in part by the Coordenação de Aperfeiçoamento de Pessoal de Nível Superior – Brasil (CAPES) – Finance Code 001.

## References

[1] United Nations, "World Population Prospects 2022: Summary of Results," United Nations, Tech. Rep., 2022. Available at: https://www.un.org/development/desa/pd/content/World-Population-Prospects-2022

[2] US Environmental Protection Agency, "GHGRP 2021: Petroleum and Natural Gas Systems," United States Environmental Protection Agency, Tech. Rep., 2021. Available at: https://www.epa.gov/ghgreporting/ghgrp-2021-petroleum-and-natural-gas-systems

[3] United Nations, "World Urbanization Prospects 2025," United Nations, Department of Economic and Social Affairs, Population Division, Tech. Rep., 2025. Available at: https://population.un.org/wup/

[4] International Energy Agency, "CCUS in Clean Energy Transitions," International Energy Agency, Energy Technology Perspectives, Tech. Rep., 2020. Available at: https://www.iea.org/reports/ccus-in-clean-energy-transitions

[5] U.S. Energy Information Administration, "Annual Energy Outlook 2020," U.S. Energy Information Administration, Tech. Rep., 2020. Available at: https://www.eia.gov/outlooks/aeo/section_issue_policies.php

[6] K. K. Chong, W. V. Grieser, A. Passman, C. H. Tamayo, N. Modeland, and B. Burke, "A completions guide book to shale-play development: A review of successful approaches towards shale-play stimulation in the last two decades," in *Canadian Unconventional Resources and International Petroleum Conference*, Calgary, Alberta, Canada, 2010, pp. SPE–133 874–MS. Available at: https://doi.org/10.2118/133874-MS

[7] T. Euzen, "Shale Gas — An Overview," IFP Technologies (Canada) Inc., Tech. Rep., 2011. Available at: https://ifp-canada.com/wp-content/uploads/2014/01/IFP_Canada_Shale_Gas_Report.pdf

[8] R. Strickland, D. Purvis, and T. Blasingame, "Practical aspects of reserve determinations for shale gas," in *North American Unconventional Gas Conference and Exhibition*, The Woodlands, Texas, USA, 2011, pp. SPE–144 357–MS. Available at: https://doi.org/10.2118/144357-MS

[9] M. Lu, Z. Pan, L. D. Connell, and Y. Lu, "A coupled, non-isothermal gas shale flow model: Application to evaluation of gas-in-place in shale with core samples," *Journal of Petroleum Science and Engineering*, vol. 158, pp. 361–379, 2017. Available at: https://doi.org/10.1016/j.petrol.2017.08.051

[10] F. A. Florence, J. A. Rushing, K. E. Newsham, and T. A. Blasingame, "Improved permeability prediction relations for low-permeability sands," in *Rocky Mountain Oil & Gas Technology Symposium*, Denver, Colorado, USA, 2007, pp. SPE–107 954–MS. Available at: https://doi.org/10.2118/107954-MS

[11] F. Civan, "Effective correlation of apparent gas permeability in tight porous media," *Transport in Porous Media*, vol. 82, no. 2, pp. 375–384, 2010. Available at: https://doi.org/10.1007/s11242-009-9432-z

[12] A. A. Moghadam and R. Chalaturnyk, "Expansion of the Klinkenberg's slippage equation to low permeability porous media," *International Journal of Coal Geology*, vol. 123, pp. 2–9, 2014. Available at: https://doi.org/10.1016/j.coal.2013.10.008

[13] F. Aminzadeh, "Hydraulic fracturing, an overview," *Journal of Sustainable Energy Engineering*, vol. 6, no. 3, pp. 204–228, 2018. Available at: https://doi.org/10.7569/jsee.2018.629512

[14] J. Taskinsoy, "Economic & ecological implications of hydraulic fracturing," *West East Journal of Social Sciences*, vol. 2, no. 1, pp. 11–39, 2013. Available at: https://www.westeastinstitute.com/journals/wp-content/uploads/2013/04/2-John-Taskinsoy-Second-paper-Ready.pdf

[15] L. Xue, C. Dai, L. Wang, and X. Chen, "Analysis of thermal stimulation to enhance shale gas recovery through a novel conceptual model," *Geofluids*, vol. 2019, no. 1, p. 4084356, 2019. Available at: https://doi.org/10.1155/2019/4084356

[16] J.-Y. Yuan, E. E. Isaacs, H. Huang, and D. G. Vandenhoff, "Wet Electric Heating Process," Patent US6 631 761B2, 2003. Available at: https://patents.google.com/patent/US6631761B2/en

[17] J. Liu, Y. Xue, Y. Fu, K. Yao, and J. Liu, "Numerical investigation on microwave-thermal recovery of shale gas based on a fully coupled electromagnetic, heat transfer, and multiphase flow model," *Energy*, vol. 263, p. 126090, 2023. Available at: https://doi.org/10.1016/j.energy.2022.126090

[18] A. K. M. Jamaluddin, D. B. Bennion, F. B. Thomas, and T. Y. Ma, "Application of heat treatment to enhance permeability in tight gas reservoirs," *Journal of Canadian Petroleum Technology*, vol. 39, no. 11, 2000. Available at: https://doi.org/10.2118/00-11-01

[19] G. Chapiro and J. Bruining, "Combustion enhance recovery of shale gas," *Journal of Petroleum Science and Engineering*, vol. 127, pp. 179–189, 2015. Available at: https://doi.org/10.1016/j.petrol.2015.01.036

[20] L. B. Lima, "Simulação numérica de escoamentos não-isotérmicos em reservatórios do tipo shale gas," Master's thesis, Instituto Politécnico, Universidade do Estado do Rio de Janeiro, Nova Friburgo, RJ, Brasil, 2023. Available at: https://www.bdtd.uerj.br/handle/1/21675

[21] T. Ertekin, J. H. Abou-Kassem, and G. R. King, *Basic Applied Reservoir Simulation*. Richardson, USA: Society of Petroleum Engineers, 2001.

[22] J. D. S. Heringer, "Simulação numérica de escoamento tridimensional não-isotérmico em reservatórios de petróleo," Master's thesis, Instituto Politécnico, Universidade do Estado do Rio de Janeiro, Nova Friburgo, RJ, Brasil, 2018. Available at: https://www.bdtd.uerj.br/handle/1/13842

[23] C. Moyne, S. Didierjean, H. P. Amaral Souto, and O. T. da Silveira, "Thermal dispersion in porous media: one-equation model," *International Journal of Heat and Mass Transfer*, vol. 43, no. 20, pp. 3853–3867, 2000. Available at: https://doi.org/10.1016/S0017-9310(00)00021-1

[24] M. Quintard and S. Whitaker, "Local thermal equilibrium for transient heat conduction: theory and comparison with numerical experiments," *International Journal of Heat and Mass Transfer*, vol. 38, no. 15, pp. 2779–2796, 1995. Available at: https://doi.org/10.1016/0017-9310(95)00028-8

[25] D. W. Peaceman, "Interpretation of well-block pressures in numerical reservoir simulation," *Society of Petroleum Engineers Journal*, vol. 18, no. 3, pp. 183–194, 1978. Available at: https://doi.org/10.2118/6893-PA

[26] H. K. Versteeg and W. Malalasekera, *An Introduction to Computational Fluid Dynamics: The Finite Volume Method*, 2nd ed. Harlow, England: Pearson Education, 2007.

[27] Z. Chen, G. Huan, and Y. Ma, *Computational Methods for Multiphase Flows in Porous Media*. Philadelphia, PA, USA: Society for Industrial and Applied Mathematics, 2006. Available at: https://doi.org/10.1137/1.9780898718942

[28] R. L. Burden and J. D. Faires, *Numerical Analysis*, 9th ed. Boston, MA, USA: Brooks/Cole, Cengage Learning, 2011.

[29] D. W. Peaceman, "Interpretation of well-block pressures in numerical reservoir simulation with nonsquare grid blocks and anisotropic permeability," *Society of Petroleum Engineers Journal*, vol. 23, no. 3, pp. 531–543, 1983. Available at: https://doi.org/10.2118/10528-PA

[30] J. G. S. Debossam, M. M. de Freitas, G. de Souza, and H. P. Amaral Souto, "Numerical simulation of three-phase flow in petroleum reservoirs using a Picard–Newton sequential method," *Journal of the Brazilian Society of Mechanical Sciences and Engineering*, vol. 47, no. 7, p. 347, 2025. Available at: https://doi.org/10.1007/s40430-025-05658-y